ACS APPLIED NANO MATERIALS
Article
Cite This: ACS Appl. Nano Mater. 2018, 1, 1641−1647
www.acsanm.org

Localized-State-Dependent Electroluminescence from ZnO/ZnS Core−Shell Nanowires−GaN Heterojunction

Ruxue Li,[†] Zhipeng Wei,[*,†] Xuan Fang,[†] Yanbin Wang,[†] Yongfeng Li,[‡] Dengkui Wang,[†] Jilong Tang,[†] Dan Fang,[†] Xueying Chu,[†] Bin Yao,[‡] Rui Chen,[*,§] and Xiaohua Wang[†]

[†]State Key Laboratory of High Power Semiconductor Lasers, School of Science, Changchun University of Science and Technology, 7089 Wei-Xing Road, Changchun 130022, P. R. China

[‡]Key Laboratory of Physics and Technology for Advanced Batteries (Ministry of Education), College of Physics, Jilin University, Changchun 130012, P. R. China

[§]Department of Electrical and Electronic Engineering, Southern University of Science and Technology, Shenzhen, Guangdong 518055, P. R. China

Supporting Information

ABSTRACT: ZnO is a very important material for excitonic ultraviolet optoelectronic devices operating above room temperature due to its wide band gap and high exciton binding energy. In this paper, the influences of different degrees of the localized state on the photoluminescence and electroluminescence properties of the ZnO/ZnS core−shell nanowires−GaN heterojunction are systematically discussed. The physical model for radiative recombination of localized carriers was proposed to explain these phenomena. Our results indicate that surface-coating of ZnS nanoparticles on ZnO nanowires (NWs) is one of the effective ways to manipulate the localized states, and only the appropriate localized state will result in the optimal optoelectronic properties.

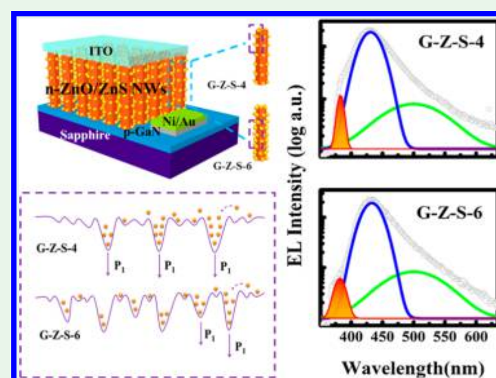

KEYWORDS: *localized excitons, ZnO/ZnS, core−shell heterostructured nanowires, interface, electroluminescence*

1. INTRODUCTION

Highly efficient ultraviolet (UV) emitters are required for applications in chemical, biological, aerospace, military, and medical technologies. Because of the wide band gap and high exciton binding energy, ZnO is considered as a suitable candidate for optoelectronic devices operating above room temperature and is a preferred material for UV optoelectronic devices.[1−7] Of the most importance for ZnO-based UV optoelectronic devices is the introduction of a suitable heterojunction and the promotion of light efficiency. However, the ZnO-based homojunction device is difficult to achieve because it is hard to fabricate stable and reproducible *p*-type ZnO. Alternatively, GaN has been chosen as the *p*-type supplement for ZnO-based optoelectronic devices,[8−10] because they have the same wurtzite crystal structure and similar lattice constant. Unfortunately, after years of investigation, this heterostructure still does not meet the requirements for practical application, which is due to its low emission efficiency and undesired emission. The low emission efficiency is due to the formation of nonradiative recombination centers at their interface.[11,12] While the undesired emission is related to weak confinement of carriers in *n*-ZnO, ZnO/GaN heterojunctions have almost the same barrier heights for electrons and holes (conduction band offset ΔE_c = 0.15 eV, valence band offset ΔE_v = 0.13 eV). Therefore, this heterojunction emits blue light rather than the ultraviolet.[13,14] For a solution to these problems, insulator layers, electron-blocking layers, hole-injection layers, etc., have been used to enhance the UV emission.[15−21] These methods indeed improve the UV emission efficiency to a certain extent, but it still needs further optimizations. Among them, the introduction of the localized state is recognized as one of the most effective ways. As is known to all, localized states are energy "traps" that are formed by fluctuations of localized potential in the band structure, which broaden the electronic density of states and are left with exponential tails in the density of states. They are created because of alloy fluctuations, interface roughness, and defects, and the optical properties of structures are strongly influenced by that. The localized states can trap free excitons to become localized excitons that show a strong carrier confinement effect.[22−24] It is reported that the exciton localization phenomenon exists in perovskite materials.[25] Moreover, Chen et al. confirmed that the localized excitons can greatly improve the emission efficiency and stability of ZnO core−shell nanowires (NWs).[26]

Received: January 23, 2018
Accepted: March 30, 2018
Published: March 30, 2018

© 2018 American Chemical Society

DOI: 10.1021/acsanm.8b00123
ACS Appl. Nano Mater. 2018, 1, 1641−1647

ZnO/ZnS is a very useful heterostructure which is able to significantly enhance the light emission of ZnO.[27] It is known that the growth of ZnS will passivate the outer surface of ZnO. Meanwhile, the wider band gap of ZnS will enhance carrier confinement. Recently, it is also noted that the introduction of ZnS sometimes will create strong carrier confinement that generates localized states.[28−32] All of these reports suggest that localized states will introduce luminescent centers for enhanced emission because they can prevent the carriers from being captured by the nonradiative recombination center. However, it is worth noting that the carriers' localized degree in ZnO core−shell NWs is sensitive to compositional or structural inhomogeneities, such as the coverage degree of ZnS nanoparticles, and they can significantly influence the optoelectronic properties. Therefore, it is highly desirable and significant, as well as a big challenge, to develop an effective and convenient method to manipulate the localized states and investigate their corresponding properties to achieve optimal performance of the UV LEDs. Unfortunately, relevant discussion is still unavailable in the literature up to now.

Here, three different degrees of localized states in the *n*-ZnO NWs−*p*-GaN heterojunction were introduced by using three corresponding coverage degrees of ZnS nanoparticles on ZnO NWs. The ZnS nanoparticles can be easily controlled by its growth cycles, and a higher coverage of ZnS nanoparticles will give rise to higher degree of localized states. Subsequently, localized-state-dependent photoluminescence (PL) and electroluminescence (EL) from this heterojunction were systematically discussed. Finally, the optimal degree of localized states has been used to demonstrate the best UV emission properties. The physical model for understanding the underlying physical mechanism of different emission properties was illustrated and discussed in detail. In addition, the light efficiency of this UV optoelectronic device is greatly improved.

2. EXPERIMENTAL SECTION

General Considerations. Zinc acetate dihydrate [$Zn(CH_3COO)_2{\cdot}2H_2O$], hexamethylenetetramine ($C_6H_{12}N_4$), sodium sulfide (Na_2S), and zinc nitrate hexahydrate [$Zn(NO_3)_2{\cdot}6H_2O$] are of analytical grade. All chemicals were used without further purification. Only when the oven achieves the predetermined temperature was the mixture put into it. Since the ZnO NWs easily adsorb impurities on the surface, the growth of ZnS nanoparticles should be carried out as soon as possible. After the completion of the growth, the samples were dried at 40 °C in the oven, and then placed in a nitrogen cabinet to prevent the samples from being contaminated.

ZnO NWs were fabricated by the chemical reaction of 0.01 mol/L $Zn(CH_3COO)_2{\cdot}2H_2O$ and 0.01 mol/L $C_6H_{12}N_4$ solution. The mixture was placed in a 25 mL Teflon-lined stainless-steel autoclave, which was then filled with solution up to 75%. The *p*-GaN/sapphire substrate is commercially available. After *p*-GaN substrate was cleaned by the conventional organic solution steps, the ZnO NWs were synthesized by typical solvothermal reactions in the oven at 95 °C for 12 h. This sample is named as G-Z.

The chemical reaction scheme and the chemical essence of the hydrothermal process synthesis are as follows: (1) Hexamethylenetetramine is used as a surfactant.

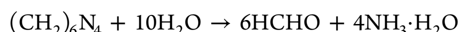

$$(CH_2)_6N_4 + 10H_2O \rightarrow 6HCHO + 4NH_3{\cdot}H_2O$$

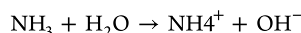

$$NH_3 + H_2O \rightarrow NH4^+ + OH^-$$

(2) The process of Zinc acetate hydrolysis follows.

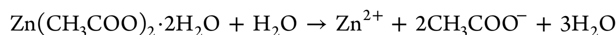

$$Zn(CH_3COO)_2{\cdot}2H_2O + H_2O \rightarrow Zn^{2+} + 2CH_3COO^- + 3H_2O$$

(3) The process of the growth of ZnO nanowires follows.

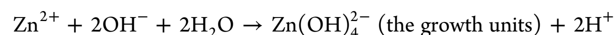

$$Zn^{2+} + 2OH^- + 2H_2O \rightarrow Zn(OH)_4^{2-} \text{ (the growth units)} + 2H^+$$

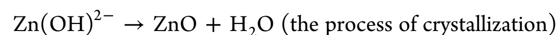

$$Zn(OH)^{2-} \rightarrow ZnO + H_2O \text{ (the process of crystallization)}$$

Moreover, the basic principle of hydrothermal process synthesis is that, first, zinc acetate is hydrolyzed to produce Zn^{2+}, and hexamethylenetetramine is hydrolyzed to form OH^-. These two kinds of ions react with water to form $Zn(OH)_4{}^{2-}$, which is the growth unit of ZnO. With the increase of the concentration of the growth units, the wafer begins crystallization of ZnO when its saturation is exceeded.

Synthesis of ZnS Nanoparticle Coating on ZnO NWs. The growth of ZnS nanoparticles was via chemical bath deposition (CBD). The as-grown ZnO NWs were immersed in 0.16 mol/L sodium sulfide (Na_2S) and zinc nitrate [$Zn(NO_3)_2$] solution for 2 h at 60 °C for completing one cycle of ZnS growth. The increase of coverage degrees of ZnS nanoparticles can be obtained by repeating the above procedures. The localized states discussed in this paper can be changed by this way. The G-Z-S-2, G-Z-S-4, and G-Z-S-6 represent samples with 2, 4, and 6 growth cycles of ZnS, respectively. Finally, all the samples were cleaned by deionized (DI) water and dried under 40 °C in an oven for further characterization. The schematics of growth processes are shown in Figure 1a−e.

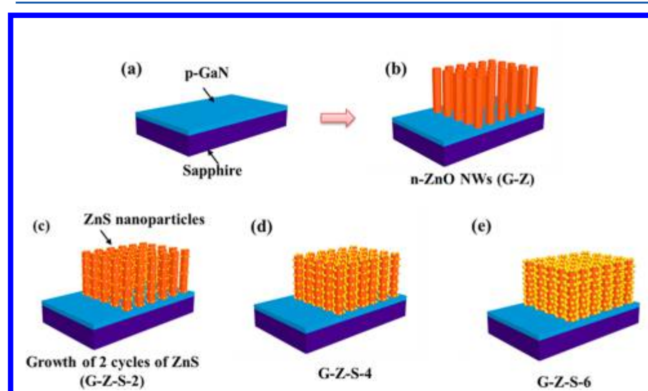

Figure 1. (a−e) Schematic growth processes.

Device Fabrication. Corresponding illustrations of light emitting diodes (LEDs) are illustrated in Figure 2a−d. The magnetron sputtering technology system was used to deposit the Ni/Au electrode on GaN. Both the Ni and Au electrode on GaN are about 50 nm, separately. The top of the ZnO nanowires was contacted with the indium tin oxide (ITO) layer, which is more conducive to light output because of its transparent structure.

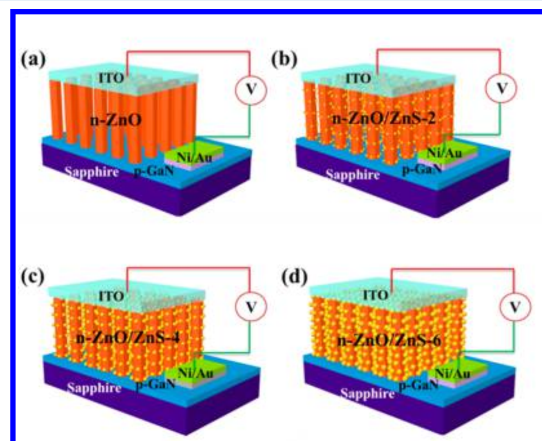

Figure 2. (a−d) Schematic of ZnO/ZnS core−shell nanowires−GaN LEDs with different coverage degrees of ZnS nanoparticles.

DOI: 10.1021/acsanm.8b00123
ACS Appl. Nano Mater. 2018, 1, 1641−1647

Characterization. A Hitachis-4800 field emission scanning electron microscope (FESEM) equipped with an energy-dispersive X-ray (EDX) spectrometer (GENE SIS 2000 XMS 60S, EDAX, Inc.) and X-ray diffraction (XRD) with a Bruker D8 advance X-ray powder diffractometer with Cu Kα radiation (λ = 1.540 981 Å) were used to characterize the composition of the samples. The transmission electron microscopy (TEM) images were obtained using a FEI Tecnai G2 F20 microscope operated at 200 kV. The HORIBA LabRAM HR Evolution instrument equipped with a He−Cd laser with line of 325 nm as the excitation source was used to perform photoluminescence (PL) measurements. The power of the excitation laser is 8 mW, and the spot size is 0.01 cm^2. Electroluminescence (EL) measurements were performed by a fluorescence meter (F4500 Hitachi).

3. RESULTS AND DISCUSSION

For an investigation of the morphology of ZnS grown on ZnO core−shell NWs, scanning electron microscopy (SEM) measurements were carried out, and the images are shown in Figure 3a−d. Compared with those of the as-grown ZnO NWs, the rough surface and the detected sulfur content (Figure S1) of the core−shell NWs indicate the successful growth of ZnS. Furthermore, it can be seen from the figures that ZnS exists as a layer of nanoparticles, and both coverage degree and sulfur content increase with the growth cycles.

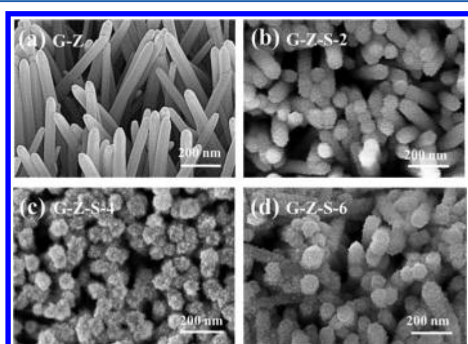

Figure 3. SEM images of as-grown ZnO NWs and the ZnO core−shell NWs with three coverage degrees of ZnS nanoparticles.

A more in-depth morphology measurement of the samples was characterized by transmission electron microscopy (TEM) and high-resolution TEM (HRTEM). As shown in Figure 4a,b, the surface of the ZnO NW is smooth, while the core−shell NW is rough (the samples of G-Z-S-2 and G-Z-S-6 have similar structure in Figure S2). In addition, in the close-up regions (insets of Figure 4c,d), the planar *d*-spacing of lattice fringes in the ZnO core is about 0.26 nm, and the shell layer is about 0.32 nm, which confirms the successful growth of ZnS.[33−35] In the HRTEM images of the core−shell NW (inset of Figure 4d), the ZnS nanoparticles and a fluctuant boundary can be clearly seen at the interface, which are marked in red dotted lines. This fluctuant boundary is ascribed to the cluster atoms between ZnO and ZnS (because of their different lattice constants), and may be the origin of the localized state.[32] For confirmation of this, temperature-dependent photoluminescence (TDPL) measurements of ZnO NWs with and without ZnS have been performed and are shown in Figure S3. The abnormal emission trend indicates the existence of carrier localization phenomenon, because, at low temperature, the emission shows an "S" shape, while at room temperature, carriers are still captured by the trap states. Therefore, it can be confirmed that localized states exist in our samples. For a deeper analysis of the structures, selected area electron diffraction (SAED) patterns are shown in Figure 4c,d. In Figure 4c, the ZnO NW possesses strong and bright diffraction spot arrays along with (002) and $(1\bar{1}0)$, implying that ZnO NW is single-crystalline in nature. In Figure 4d, the core−shell NW has much weaker and blurrier diffraction spots on the diffraction circles of ZnS (111), (220), and (311), indicating that the ZnS layer is polycrystalline.[36−38] In addition, the strong diffraction spot arrays of ZnO (002) and $(1\bar{1}0)$ still exist in Figure 4d, implying that the ZnO core still holds a better crystal quality in the core−shell NWs. These results are in accordance with X-ray diffraction (XRD) data in Figure S4. With the increase of the ZnS nanoparticle, the diffraction intensity of ZnS (111) will increase, and the full width at half-maximum (fwhm) will decrease accordingly.[32] It is easier for the polycrystalline structure to create localized fluctuations at the interface, and it is reported in ref 32 that the higher degrees of fluctuations of atoms at the interface give rise to the higher degree of localized states. Therefore, the degree of localized state in our paper will show a linear relationship with the coverage degree of ZnS nanoparticles.

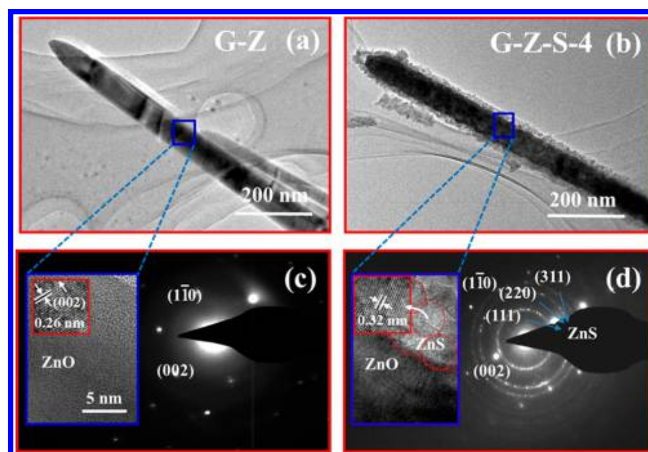

Figure 4. TEM images of individual NWs of the (a) G-Z sample, and (b) G-Z-S-4 sample. (c, d) SAED patterns from the ZnO NWs and G-Z-S sample in parts a and b. The insets are corresponding HRTEM images of G-Z and G-Z-S-4, and the close-up photographs are the planar *d*-spacing of lattice fringes of ZnO NW and ZnS nanoparticles, respectively. The ZnS nanoparticles are marked in red dotted circles, and the fluctuate boundary at the interface of ZnO and ZnS is marked in a red dotted line.

According to the SEM and TEM results, the transformations of the morphologies of core−shell NWs are intrinsically the evolutions of the coverage degree of ZnS nanoparticles. These transformations will result in the change of localized state, which will affect their optoelectronic properties. For an investigation of the influence of different localized states on the optical property of ZnO/ZnS core−shell NWs, room-temperature−PL (RT−PL) measurements were performed. As shown in Figure 5, the peak position of the UV emission located at 382.5 nm is ascribed to the near-band-edge (NBE) emission from ZnO,[6] while the peak position centered at approximately 550 nm comes from the deep level emission (DLE).[26,34,39,40] After the introduction of ZnS nanoparticles onto the ZnO NWs, the core−shell samples show similar UV emission.[41] It is reported that the localized states can provide luminescent centers and prevent the carriers from being captured by nonradiative recombination centers to enhance the UV emission.[22−26] Therefore, as shown in inset of Figure 5, the fwhm of the UV emissions monotonously increase, which indicates that the luminescent centers have increased and that

DOI: 10.1021/acsanm.8b00123
ACS Appl. Nano Mater. 2018, 1, 1641−1647

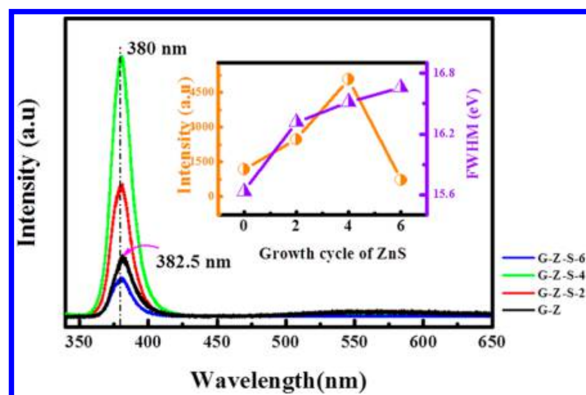

Figure 5. RT−PL spectra of G-Z, G-Z-S-2, G-Z-S-4, and G-Z-S-6 samples. The inset is the value of the peak intensity and the fwhm of different samples.

the structures are more inhomogeneous. For the UV intensity, it shows the trend of increasing first and then decreasing; namely, the PL intensity from the G-Z-S-6 (with highest degree of localized state) is the weakest, which implies that there are different physical mechanisms of the emission. In the sample of G-Z-S-2, the defect and surface states of ZnO NWs will not be fully passivated, which gives rise to the weak emission. With the increase of ZnS, more and more defects and surface states of ZnO NWs are modified, and the localized states are sufficient to trap more injected carriers from diffusing to nonradiative recombination centers. Therefore, the intensity of the device emission increases. However, with more growth cycles, the ZnS nanoparticles will form a layer and bring some other defects near the structure. Therefore, the PL intensity increases first and then decreases.

For a further investigation of the physical mechanisms, EL spectra of the devices are shown in Figure 6, which were

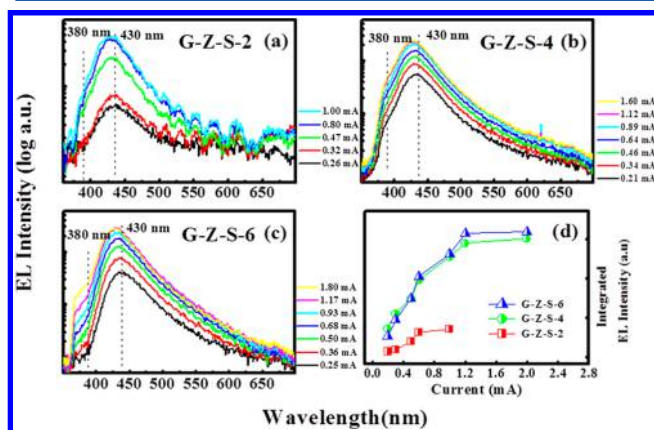

Figure 6. (a−c) RT−EL spectra of corresponding LEDs of G-Z-S-2, G-Z-S-4, and G-Z-S-6 were added with injection currents of 0.2−1 mA under forward bias. (d) Diagram of the integrated EL intensity of each G-Z-S sample.

measured under forward bias with injection currents from 0.2 to 1 mA at RT. Compared with the G-Z sample which only emits at 430 nm (Figure S5), all the G-Z-S samples obviously show 380 nm emissions, implying that it does not come intrinsically from the ZnO, but should be ascribed to the emission near the ZnO/ZnS interface.[13,14] These UV emissions are ascribed to strong localization of carriers in the ZnO surface, which shows the electron-blocking ability in the ZnO/ZnS core−shell NWs−GaN heterojunction. Moreover, it is important to note that the EL intensity of the G-Z-S samples is much higher than that of G-Z, and therefore, the localized states also exhibit the ability of providing luminescent centers. However, from both the PL and EL measurements, the intensity of the G-Z-S-4 is the highest. The main reason for this observation is that the degrees of the localized states in G-Z-S-2 are low, while they are extremely high for G-Z-S-6. It is known that EL and PL may be different because their excitation situation is different. EL needs to consider the carrier diffusion, while PL needs to consider which part has been excited. In our case, the carrier diffusion will happen near the interface of NWs and GaN, while the injected carriers will diffuse from GaN to NWs; therefore, the emission band of EL is more sensitive to interface defects. Different ZnS coatings will lead to the change of defect states, surface states, and localized states, and the EL is the result of the competition between them. In the sample of G-Z-S-2, the defect states and surface states of ZnO NWs will not be fully passivated. Therefore, the carriers will diffuse to nonradiative recombination which leads to a weak emission. Furthermore, other supporting information for this claim will be provided and discussed later.

For a deep analysis of this phenomenon, EL spectra of the G-Z-S samples under different injection currents were fitted by three Gaussian peaks. As shown in Figure 7, they are marked by

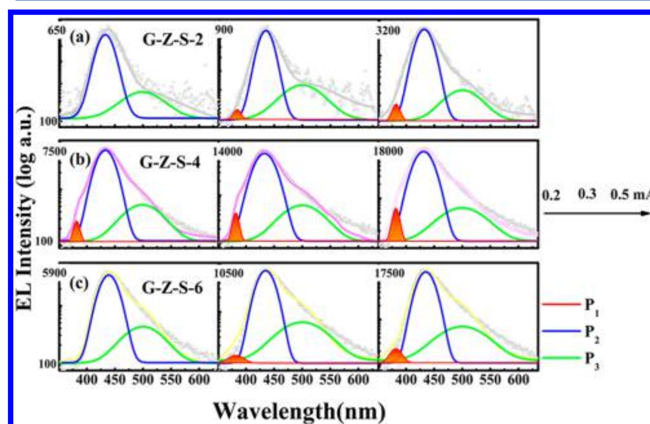

Figure 7. (a−c) EL Gaussian fitting spectra in different injection currents (0.2−0.5 mA) of G-Z-S-2, G-Z-S-4, and G-Z-S-6, respectively. The P_1, P_2, and P_3 represent the emission of ZnO, GaN, and defect, respectively.

red, blue, and green, which are located at 380, 430, and about 500 nm, respectively. Compared with the G-Z sample and some reports on EL from this *n*-ZnO NWs−*p*-GaN structure, the peaks are ascribed to ZnO, GaN, and defect emission, respectively.[11,15−21,42,43] The EL intensity of both the G-Z sample and these reports are very weak and lack the UV emission from ZnO NWs. Therefore, among them, the evolution of the UV emission (the red filled area) is the most important for discussion of localized states. From Figure 7, it can be seen that, with the increase of injection current, the intensity of the UV emission becomes stronger, implying that the number of injection carriers which are captured by localized states increases. However, as shown in Figure 8a, the UV emission only appears in the G-Z-S-4 at low injection current of 0.2 mA, and the UV intensity of it is the highest even under high injection current. This may be the reason that the degree of localized states in the G-Z-S-4 is optimal, and there is a

DOI: 10.1021/acsanm.8b00123
ACS Appl. Nano Mater. 2018, 1, 1641−1647

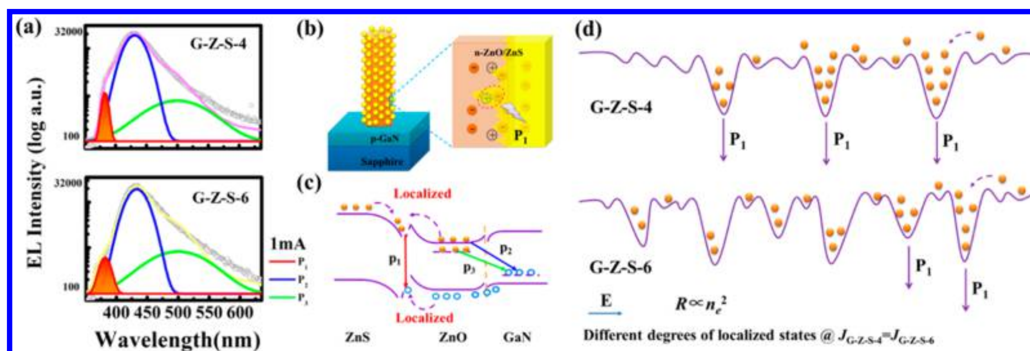

Figure 8. (a) EL Gaussian fitting spectra of G-Z-S-4 and G-Z-S-6 at 1 mA. (b) Schematic diagram of ZnO/ZnS core−shell nanowires−GaN heterojunction in this paper. (c) Energy band schematic diagram of the G-Z-S sample. (d) Different degrees of localized states and the radiative recombination mechanism of different degrees of localized states.

competition between radiative and nonradiative recombination in the samples. A clearer description will be presented in the following analysis.

For the LED devices, the injection carriers would undergo both radiative and nonradiative recombination when they pass through the *p*−*n* junction. The radiative recombination is responsible for emission, while the nonradiative recombination will result in thermal radiation. For the ZnO/ZnS core−shell nanowires−GaN heterojunction (schematic diagram is drawn in Figure 8b), the fluctuant boundary between ZnO core and ZnS shell induces the localized states. The localized state has the ability of strong carrier confinement and can trap carriers from diffusing to nonradiative recombination centers. Therefore, the EL intensity of the G-Z sample is much weaker than those of the G-Z-S. The radiative recombination of the G-Z-S mainly comes from three mechanisms, which have been schematically described by the energy band diagram plotted in Figure 8c. They correspond to the emission of the ZnO, GaN, and defect in Figure 8a, and are denoted by P_1, P_2, and P_3, respectively. From the figure, the barrier height of the ZnO/GaN heterojunctions is almost the same, which will result in a weak confinement of carriers in ZnO. Therefore, if no localized states exist, there will be only P_2 and P_3 emission from the heterojunction.[13,14] The introduction of ZnS nanoparticles can cause energy traps (the localized states) at the interface between the ZnO core and ZnS shell, which will capture the carriers to form the P_1 transition, as shown in Figure 8b,c. The different degrees of the localized state are vividly shown in Figure 8d.[30] This shows that higher degree of localized states will have higher density of energy traps, which will capture more carriers and thus lead to enhanced emission. However, according to the PL and EL results, the intensity of emission of these samples does not linearly increase, and it has been shown that the G-Z-S-4 sample exhibits the best optoelectronic properties. Therefore, the model describes the radiative recombination of the semiconductor, and a competition between radiative and nonradiative recombination can be used to explain these phenomena.

The radiative recombination is more preferred for the LED. However, nonradiative recombination always coexists in devices. Thus, there is a competition between radiative and nonradiative recombination. It is noted that the increase of the radiative process and decrease of the nonradiative process will be good for device applications. It was reported that the ZnS layer has the abilities of both the introduction of localized state and the passivation of surface state. The different coatings of ZnS will lead to the change of defect states, surface states, and localized states. Therefore, EL is the result of the competition of the three. The surface state will be responsible for nonradiative recombination. It can be concluded that the surface coverage of G-Z-S-2 is too low to passivate all of the surface defects. This is why its UV emission could not be observed under very small injection current (Figure 7a). With the increase of ZnS growth cycles, more and more defects and surface states of ZnO NWs are passivated, while localized states can trap more carriers from diffusing to nonradiative recombination centers. Therefore, the intensity of emission increases. Thus, for the G-Z-S-4 and G-Z-S-6 samples, the surface passivation is effective, and they have shown a very intensive emission. However, with the growth of ZnS, more and more defects will be created because of its polycrystalline nature. For quantification of the radiative recombination of ultraviolet emission in G-Z-S-4 and G-Z-S-6, the bimolecular rate equation of radiative recombination in a semiconductor can be used:[44,45]

$$R = -\frac{dn_e}{dt} = -\frac{dn_h}{dt} = Bn_e n_h \quad (1)$$

where R is the radiative recombination rate, n_e the electron concentration, n_h the hole concentration, and B the radiative recombination coefficient, whose typical values are from about 10^{-11} to 10^{-9} cm^3/s for ZnO.[46,47] Since excess carriers are generated and recombined in pairs (namely, $n_e = n_h$), eq 1 becomes $R = Bn_e^2$. This equation implies that the radiative recombination rate R in each localized trap is proportional to the square of the carrier concentration, which means that the high localized carrier concentration will lead to a high radiative recombination rate and thus intensive emission. Therefore, the UV intensity of G-Z-S-6 is weaker than that of G-Z-S-4 under the same injection current, which is because the localized carrier concentration decreases with the increase of the localized states' density of state (DOS), as shown in Figure 8d. The G-Z-S-6 has the higher localized states' density of state as compared to G-Z-S-4, and as a result the average number of carriers in each trap is less than G-Z-S-4 under the same injection current. In addition, the more localized traps in G-Z-S-6 will lead to wider fwhm values of the emission. Finally, the degree of the localized states in the G-Z-S-4 is optimal.

4. CONCLUSION

In conclusion, different degrees of the localized state were successfully introduced to the ZnO NWs. It was found that higher surface coverage of ZnS nanoparticles will give rise to

DOI: 10.1021/acsanm.8b00123
ACS Appl. Nano Mater. 2018, 1, 1641−1647

higher degree of localized states. The PL and the EL results reveal that localized states can significantly influence the optoelectronic properties and is beneficial for emission. From the bimolecular radiative recombination rate of localized states, it can be seen that when the concentration of localized carriers is higher, the luminescence is better. In addition, the localized carrier concentration decreases with the increase of the localized states' density of state. Therefore, extremely high density of the localized states (G-Z-S-6) is unfavorable for intensive UV emission, although most of its surface states have been passivated. Last but not least, the introduced localized state of G-Z-S-4 is optimal, and only the appropriate localized states will result in the best optoelectronic properties. This demonstrates that manipulation of localized states and study of their corresponding properties in the ZnO/ZnS core−shell nanowires−GaN heterojunction are significant for their device applications. The methods will provide useful references for other materials and promote the developing of high-performance optoelectronic devices based on localized state.

ASSOCIATED CONTENT

Supporting Information

The Supporting Information is available free of charge on the ACS Publications website at DOI: 10.1021/acsanm.8b00123.

Additional illustration of the EDS results, TEM images, temperature-dependent peak positions, XRD patterns, and RT−EL spectra (PDF)

AUTHOR INFORMATION

Corresponding Authors

*E-mail: zpweicust@126.com.
*E-mail: chen.r@sustc.edu.cn.

ORCID

Xuan Fang: 0000-0003-2290-4951
Yongfeng Li: 0000-0002-9725-0692
Bin Yao: 0000-0003-0748-3220
Rui Chen: 0000-0002-0445-7847

Author Contributions

The manuscript was written through contributions of all authors. All authors have given approval to the final version of the manuscript.

Notes

The authors declare no competing financial interest.

ACKNOWLEDGMENTS

This work is supported by the National Natural Science Foundation of China (11574130, 11404161, 61404009, 61474010, 61574022, 61504012, 61674021, 11404219, and 11674038), the Developing Project of Science and Technology of Jilin Province (20160519007JH, 20160520117JH, 20160101255JC, 20160204074GX, 20170520117JH, and 20170520118JH). R.C. acknowledges the support from national 1000 plan for young talents and Shenzhen Science and Technology Innovation Committee (Projects: KQJSCX20170726145748464, JCYJ20150930160634263, and KQTD2015071710313656).

ABBREVIATIONS

UV = ultraviolet
SEM = scanning electron microscopy
TEM = transmission electron microscopy
HRTEM = high-resolution TEM
NWs = nanowires
TDPL = temperature-dependent photoluminescence
SAED = selected area electron diffraction
XRD = X-ray diffraction
RT = room temperature
PL = photoluminescence
NBE = near-band-edge
DLE = deep level emission
fwhm = full width at half-maximum
DOS = density of state

REFERENCES

(1) Lu, J. F.; Shi, Z. L.; Wang, Y. Y.; Lin, Y.; Zhu, Q. X.; Tian, Z. S.; Dai, J.; Wang, S. F.; Xu, C. X. Plasmon-enhanced Electrically Light-emitting from ZnO Nanorod Arrays/p-GaN Heterostructure Devices. *Sci. Rep.* **2016**, *6*, 25645.

(2) Wang, Z. N.; Yu, R. M.; Pan, C. F.; Li, Z. L.; Yang, J.; Yi, F.; Wang, Z. L. Light-induced Pyroelectric Effect as an Effective Approach for Ultrafast Ultraviolet Nanosensing. *Nat. Commun.* **2015**, *6*, 8401.

(3) Han, X.; Du, W. M.; Yu, R. M.; Pan, C. F.; Wang, Z. L. Piezo-Phototronic Enhanced UV Sensing Based on a Nanowire Photodetector Array. *Adv. Mater.* **2015**, *27*, 7963−7969.

(4) Chu, S.; Wang, G. P.; Zhou, W. H.; Lin, Y. Q.; Chernyak, L.; Zhao, J. Z.; Kong, J. Y.; Li, L.; Ren, J. J.; Liu, J. J. Electrically Pumped Waveguide Lasing from ZnO Nanowires. *Nat. Nanotechnol.* **2011**, *6*, 506−510.

(5) Bie, Y. Q.; Liao, Z. M.; Zhang, H. Z.; Li, G. R.; Ye, Y.; Zhou, Y. B.; Xu, J.; Qin, Z. X.; Dai, L.; Yu, D. P. Self-Powered, Ultrafast, Visible-Blind UV Detection and Optical Logical Operation based on ZnO/GaN Nanoscale p-n Junctions. *Adv. Mater.* **2011**, *23*, 649−653.

(6) Lupan, O.; Pauporté, T.; Bruno, V. Low-Voltage UV-Electroluminescence from ZnO-Nanowire Array/p-GaN Light-Emitting diodes. *Adv. Mater.* **2010**, *22*, 3298−3302.

(7) Nie, Y.; Wang, Z.; Wang, J.; Bao, F.; Zhang, J.; Ma, Y.; Sham, T.-K.; Sun, X. Synthesis and Structure-Dependent Optical Properties of ZnO Nanocomb and ZnO Nanoflag. *J. Phys. Chem. C* **2017**, *121*, 26076−26085.

(8) Choi, J. H.; Kim, J.; Yoo, H.; Liu, J.; Kim, S.; Baik, C. W.; Cho, C. R.; Kang, J. G.; Kim, M.; Braun, P. V.; Hwang, S.; Jung, T. S. Heteroepitaxial Growth of GaN on Unconventional Templates and Layer-Transfer Techniques for Large-Area, Flexible/Stretchable Light-Emitting Diodes. *Adv. Opt. Mater.* **2016**, *4*, 505−521.

(9) Schuster, F.; Laumer, B.; Zamani, R. R.; Magén, C.; Morante, J. R.; Arbiol, J.; Stutzmann, M. p-GaN/n-ZnO Heterojunction Nanowires: Optoelectronic Properties and the Role of Interface Polarity. *ACS Nano* **2014**, *8*, 4376−4384.

(10) Vispute, R. D.; Talyansky, V.; Choopun, S.; Sharma, R. P.; Venkatesan, T.; He, M.; Tang, X.; Halpern, J. B.; Spencer, M. G.; Li, Y. X.; Salamanca-Riba, L. G.; Iliadis, A. A.; Jones, K. A. Heteroepitaxy of ZnO on GaN and Its Implications for Fabrication of Hybrid Optoelectronic Devices. *Appl. Phys. Lett.* **1998**, *73*, 348.

(11) Alivov, Y. I.; Van-Nostrand, J. E.; Look, D. C.; Chukichev, M. V.; Ataev, B. M. Observation of 430 nm Electroluminescence From ZnO/GaN Heterojunction Light-emitting Diodes. *Appl. Phys. Lett.* **2003**, *83*, 2943.

(12) You, J. B.; Zhang, X. W.; Zhang, S. G.; Wang, J. X.; Yin, Z. G.; Tan, H. R.; Zhang, W. J.; Chu, P. K.; Cui, B. A.; Wowchak, M.; Dabiran, A. M.; Chow, P. P. Improved Electroluminescence from n-ZnO/AlN/p-GaN Heterojunction Light-emitting Diodes. *Appl. Phys. Lett.* **2010**, *96*, 201102.

(13) Zhang, L. C.; Li, Q. S.; Shang, L.; Wang, F. F.; Qu, C.; Zhao, F. Z. Improvement of UV Electroluminescence of n-ZnO/p-GaN Heterojunction LED by ZnS Interlayer. *Opt. Express* **2013**, *21*, 16578−16583.

(14) Wang, S.; Wang, L. W. Atomic and Electronic Structures of GaN/ZnO Alloys. *Phys. Rev. Lett.* **2010**, *104*, 065501.

(15) Zhang, C.; Zhang, J.; Liu, W. Z.; Xu, H. Y.; Hou, S.; Wang, C. L.; Wang, Z. Q.; Wang, X. H.; Liu, Y. C. Enhanced Ultraviolet Random Lasing from Au/MgO/ZnO Heterostructure by Introducing p-Cu_2O Hole-injection Layer. *ACS Appl. Mater. Interfaces* **2016**, *8*, 31485−31490.
(16) Liu, Y. C.; Xu, H. Y.; Liu, C. Y.; Liu, W. Z. Recent Progress in ZnO-based Heterojunction Ultraviolet Light-emitting Devices. *Chin. Sci. Bull.* **2014**, *59*, 1219−1227.
(17) Zhang, S. G.; Zhang, X. W.; Yin, Z. G.; Wang, J. X.; Si, F. T.; Gao, H. L.; Dong, J. J.; Liu, X. Optimization of Electroluminescence from n-ZnO/AlN/p-GaN Light-emitting Diodes by Tailoring Ag Localized Surface Plasmon. *J. Appl. Phys.* **2012**, *112*, 013112.
(18) Li, S. Z.; Fang, G. J.; Long, H.; Wang, H. N.; Huang, H. H.; Mo, X. M.; Zhao, X. Z. Low-threshold Pure UV Electroluminescence from n-ZnO: Al/i-layer/n-GaN Heterojunction. *J. Lumin.* **2012**, *132*, 1642−1645.
(19) Zhang, X. M.; Lu, M. Y.; Zhang, Y.; Chen, L. J.; Wang, Z. L. Fabrication of a High-Brightness Blue-Light-Emitting Diode Using a ZnO-Nanowire Array Grown on p-GaN Thin Film. *Adv. Mater.* **2009**, *21*, 2767−2770.
(20) Jeong, M. C.; Oh, B. Y.; Ham, M. H.; Lee, S. W.; Myoung, J. M. ZnO-Nanowire-Inserted GaN/ZnO Heterojunction Light-Emitting Diodes. *Small* **2007**, *3*, 568−572.
(21) Park, W. I.; Yi, G. C. Electroluminescence in n-ZnO Nanorod Arrays Vertically Grown on p-GaN. *Adv. Mater.* **2004**, *16*, 87−90.
(22) Li, Q.; Xu, S. J.; Xie, M. H.; Tong, S. Y. A Model for Steady-state Luminescence of Localized-State Ensemble. *Europhys. Lett.* **2005**, *71*, 994.
(23) Li, Q.; Xu, S. J.; Xie, M. H.; Tong, S. Y. Origin of the 'S-shaped' Temperature Dependence of Luminescent Peaks from Semiconductors. *J. Phys.: Condens. Matter* **2005**, *17*, 4853.
(24) Cho, Y. H.; Gainer, G. H.; Fischer, A. J.; Song, J. J.; Keller, S.; Mishra, U. K.; DenBaars, S. P. S-shaped" Temperature-dependent Emission Shift and Carrier Dynamics in InGaN/GaN Multiple Quantum Wells. *Appl. Phys. Lett.* **1998**, *73*, 1370−1372.
(25) He, H. P.; Yu, Q. Q.; Li, H.; Li, J.; Si, J. J.; Jin, Y. Z.; Wang, N. N.; Wang, J. P.; He, J. W.; Wang, X. K.; Zhang, Y.; Ye, Z. Z. Exciton Localization in Solution-processed Organolead Trihalide Perovskites. *Nat. Commun.* **2016**, *7*, 10896.
(26) Chen, R.; Ye, Q. L.; He, T. C.; Ta, V. D.; Ying, Y. J.; Tay, Y. Y.; Wu, T.; Sun, H. Exciton Localization and Optical Properties Improvement in Nanocrystal-embedded ZnO Core-Shell Nanowires. *Nano Lett.* **2013**, *13*, 734−739.
(27) Li, J. H.; Zhao, D. X.; Meng, X. Q.; Zhang, Z. Z.; Zhang, J. Y.; Shen, D. Z.; Lu, Y. M.; Fan, X. W. Enhanced Ultraviolet Emission from ZnS-Coated ZnO Nanowires Fabricated by Self-Assembling Method. *J. Phys. Chem. B* **2006**, *110*, 14685.
(28) Fang, X.; Wei, Z. P.; Chen, R.; Tang, J. L.; Zhao, H. F.; Zhang, L. G.; Zhao, D. X.; Fang, D.; Li, J. H.; Fang, F.; Chu, X. Y.; Wang, X. H. Influence of Exciton Localization on the Emission and Ultraviolet Photoresponse of ZnO/ZnS Core-Shell Nanowires. *ACS Appl. Mater. Interfaces* **2015**, *7*, 10331−10336.
(29) Fang, X.; Wei, Z. P.; Yang, Y. H.; Chen, R.; Li, Y. F.; Tang, J. L.; Fang, D.; Jia, H. M.; Wang, D. K.; Fan, J.; Ma, X. H.; Yao, B.; Wang, X. H. Ultraviolet Electroluminescence from ZnS@ZnO Core-Shell Nanowires/p-GaN Introduced by Exciton Localization. *ACS Appl. Mater. Interfaces* **2016**, *8*, 1661−1666.
(30) Wang, H. N.; Ji, Z. W.; Qu, S.; Wang, G.; Jiang, Y. Z.; Liu, B. L.; Xu, X. G.; Mino, H. Influence of Excitation Power and Temperature on Photoluminescence in InGaN/GaN Multiple Quantum Wells. *Opt. Express* **2012**, *20*, 3932−3940.
(31) Zhu, H.; Shan, C. X.; Li, B. H.; Zhang, Z. Z.; Zhang, J. Y.; Yao, B.; Shen, D. Z.; Fan, X. W. Enhanced Photoluminescence Caused by Localized Excitons Observed in MgZnO Alloy. *J. Appl. Phys.* **2009**, *105*, 103508.
(32) Li, R. X.; Wei, Z. P.; Zhao, F. H.; Gao, X.; Fang, X.; Li, Y. F.; Wang, X. W.; Tang, J. L.; Fang, D.; Wang, H. Z.; Chen, R.; Wang, X. H. Investigation of Localized and Delocalized Excitons in ZnO/ZnS Core-shell Heterostructured Nanowires. *Nanophotonics* **2017**, *6*, 1093.
(33) Hu, H. B.; Wang, K.; Long, H.; Liu, W. W.; Wang, B.; Lu, P. Precise Determination of the Crystallographic Orientations in Single ZnS Nanowires by Second-harmonic Generation Microscopy. *Nano Lett.* **2015**, *15*, 3351−3357.
(34) Bera, A.; Basak, D. Photoluminescence and Photoconductivity of ZnS-coated ZnO nanowires. *ACS Appl. Mater. Interfaces* **2010**, *2*, 408−412.
(35) Chen, R.; Li, D. H.; Liu, B.; Peng, Z. P.; Gurzadyan, G. G.; Xiong, Q. H.; Sun, H. D. Optical and Excitonic Properties of Crystalline ZnS Nanowires: Toward Efficient Ultraviolet Emission at Room Temperature. *Nano Lett.* **2010**, *10*, 4956−4961.
(36) Shuai, X. M.; Shen, W. Z. A Facile Chemical Conversion Synthesis of ZnO/ZnS Core/Shell Nanorods and Diverse Metal Sulfide Nanotubes. *J. Phys. Chem. C* **2011**, *115*, 6415−6422.
(37) Hu, Y.; Qian, H.; Liu, Y.; Du, G. H.; Zhang, F. M.; Wang, L. B.; Hu, X. A Microwave-Assisted Rapid Route to Synthesize ZnO/ZnS Core-Shell Nanostructures via Controllable Surface Sulfidation of ZnO Nanorods. *CrystEngComm* **2011**, *13*, 3438−3443.
(38) Lupan, O.; Pauporté, T.; Le-Bahers, T.; Viana, B.; Ciofini, I. Wavelength-emission Tuning of ZnO Nanowire-based Light-Emitting Diodes by Cu Doping: Experimental and Computational Insights. *Adv. Funct. Mater.* **2011**, *21*, 3564−3572.
(39) Chen, R.; Ye, Q. L.; He, T. C.; Wu, T.; Sun, H. D. Uniaxial Tensile Strain and Excitons-Phonon Coupling in Bent ZnO Nanowires. *Appl. Phys. Lett.* **2011**, *98*, 241916.
(40) Hsu, C. L.; Chang, S. J. Doped ZnO 1D Nanostructures: Synthesis, Properties, and Photodetector Application. *Small* **2014**, *10*, 4562−4585.
(41) Guo, P. H.; Jiang, J. G.; Shen, S. H.; Guo, L. J. ZnS/ZnO Heterojunction as Photoelectrode: Type II Band Alignment Towards Enhanced Photoelectrochemical Performance. *Int. J. Hydrogen Energy* **2013**, *38*, 13097−13103.
(42) Rogers, D. J.; Teherani, F. H.; Yasan, A.; Minder, K.; Kung, P.; Razeghi, M. Electroluminescence at 375 nm from a ZnO/GaN: Mg/c-Al_2O_3 Heterojunction Light Emitting Diode. *Appl. Phys. Lett.* **2006**, *88*, 141918.
(43) Yang, Q.; Wang, W. H.; Xu, S.; Wang, Z. L. Enhancing Light Emission of ZnO Microwire-Based Diodes by Piezo-Phototronic Effect. *Nano Lett.* **2011**, *11*, 4012−4017.
(44) Schubert, E. F. In *Light Emitting Diodes*; Cambridge University Press: Cambridge, 2003; Chapter 2, pp 27−31.
(45) Dai, Q.; Schubert, M. F.; Kim, M. H.; Kim, J. K.; Schubert, E. F.; Koleske, D. D.; Crawford, M. H.; Lee, S. R.; Fischer, A. J.; Thaler, G.; Banas, M. A. Internal Quantum Efficiency and Nonradiative Recombination Coefficient of GaInN/GaN Multiple Quantum Wells with Different Dislocation Densities. *Appl. Phys. Lett.* **2009**, *94*, 111109.
(46) Trupke, T.; Green, M. A.; Wurfel, P.; Altermatt, P. P.; Wang, A.; Zhao, J.; Corkish, R. Temperature Dependence of the Radiative Recombination Coefficient of Intrinsic Crystalline Silicon. *J. Appl. Phys.* **2003**, *94*, 4930.
(47) Schenk, H. P. D.; Borenstain, S. I.; Berezin, A.; Schön, A.; Cheifetz, E.; Dadgar, A.; Krost, A. Cathodoluminescence of Epitaxial GaN and ZnO Thin Films for Scintillator Applications. *J. Cryst. Growth* **2009**, *311*, 3984−3988.

DOI: 10.1021/acsanm.8b00123
ACS Appl. Nano Mater. 2018, 1, 1641−1647